OXFORD

Integrative Biology, 2021, 13(5),109–120

doi: 10.1093/intbio/zyab006
Advance Access publication April 24, 2021
Original Article

ORIGINAL ARTICLE

Mechanistic dissection of spatial organization in NF-κB signaling pathways by hybrid simulations

Yinghao Wu*, Kalyani Dhusia, and Zhaoqian Su

Department of Systems and Computational Biology, Albert Einstein College of Medicine, Bronx, NY, USA

***Corresponding author**. E-mail: yinghao.wu@einsteinmed.org

Abstract

The nuclear factor kappa-light-chain-enhancer of activated B cells (NF-κB) is one of the most important transcription factors involved in the regulation of inflammatory signaling pathways. Inappropriate activation of these pathways has been linked to autoimmunity and cancers. Emerging experimental evidences have been showing the existence of elaborate spatial organizations for various molecular components in the pathways. One example is the scaffold protein tumor necrosis factor receptor associated factor (TRAF). While most TRAF proteins form trimeric quaternary structure through their coiled-coil regions, the N-terminal region of some members in the family can further be dimerized. This dimerization of TRAF trimers can drive them into higher-order clusters as a response to receptor stimulation, which functions as a spatial platform to mediate the downstream poly-ubiquitination. However, the molecular mechanism underlying the TRAF protein clustering and its functional impacts are not well-understood. In this article, we developed a hybrid simulation method to tackle this problem. The assembly of TRAF-based signaling platform at the membrane-proximal region is modeled with spatial resolution, while the dynamics of downstream signaling network, including the negative feedbacks through various signaling inhibitors, is simulated as stochastic chemical reactions. These two algorithms are further synchronized under a multiscale simulation framework. Using this computational model, we illustrated that the formation of TRAF signaling platform can trigger an oscillatory NF-κB response. We further demonstrated that the temporal patterns of downstream signal oscillations are closely regulated by the spatial factors of TRAF clustering, such as the geometry and energy of dimerization between TRAF trimers. In general, our study sheds light on the basic mechanism of NF-κB signaling pathway and highlights the functional importance of spatial regulation within the pathway. The simulation framework also showcases its potential of application to other signaling pathways in cells.

Key words: NF-κB signaling pathways; hybrid simulations; ligand–receptor oligomerization

INSIGHT BOX

The NF-κB signaling pathway is a signaling pathway regulating inflammatory responses. Recent experiments showed that the molecular components in the pathway can organize into high-order structures in cells. However, the molecular mechanism of these spatial organization and their functional impacts remain unclear. Here, we developed a new computational method to tackle this problem. Using this method, we demonstrated that the assembly of high-order spatial structure is a critical factor to regulate the downstream oscillatory dynamics in the NF-κB signaling network. Interestingly, mutations either weaken or strengthen the assembly can cause the abolishment of oscillation in the pathway. This observation suggests that molecular elements and their interactions in a signaling network are elaborately designed to carry out their appropriate functions.

Received November 12, 2020; **accepted** March 29, 2021

INTRODUCTION

The innate immune system constitutes the first line of host defense during infections by invading pathogens [1]. This defensive response, called inflammation, is a complicated process orchestrated by many different cellular components [2, 3]. At the onset of inflammation, cytokines are released from immune cells, such as macrophage, after they capture infected cells [2]. The nuclear factor kappa-light-chain-enhancer of activated B cells (NF-κB) is a critical transcription factor, which regulates the expressions of cytokines that stimulate inflammatory responses [4, 5]. Under normal condition, NF-κB is retained in the cytoplasm with an inhibitory factor, IκB [6, 7]. The NF-κB activation is started from the binding of membrane receptors, mainly in tumor necrosis factor (TNF) receptor superfamily to their extracellular ligands [8]. The ligand binding of receptors triggers the recruitment of adaptor proteins, such as TNF receptor-associated factor (TRAF), to their cytoplasmic domains [9]. Although the C-terminal domain of TRAF maintains interactions with upstream receptors, the N-terminal regions function as platform to mediate the process of poly-ubiquitination [10]. The ubiquitination leads to the degradation of IκB, so that NF-κB can be released and enter cell nucleus to initiate gene expression [11, 12]. It has been found that spatial organizations of proteins are highly involved in signaling pathways [13, 14]. Such phenomena have also been observed in NF-κB signaling pathway [15]. For instance, *in vivo* experiments have shown that TRAF proteins can aggregate to higher-order spatial patterns as a response to receptor stimulation [16, 17]. The structural evidences further indicate that the N-terminal region in some TRAF proteins, such as TRAF6 and TRAF2, is dimeric [16, 18, 19]. The capability of high-order pattern formation can be abolished by a mutant that disables this dimerization. As a result, it was proposed that the dimerization can lead to a 2D clustering of trimeric TRAF protein complexes. However, it is not fully understood how this spatial organization regulates the dynamics in NF-κB signaling pathway.

Due to the functional importance of NF-κB in immunity, the molecular mechanisms of its signaling pathway are under intensive investigation [20]. Comparing with other traditional wet-laboratory experiments, computational modeling is more convenient to explore the complexity of a biological system on a mechanistic level. As a result, a large variety of models have been developed on different scales of the pathway. The original model focused on the role of IκB in regulating the temporal dynamics of NF-κB by using a set of ordinary differential equations (ODE) [21, 22]. More recently, stochastic simulations and agent-based modeling (ABM) approaches were applied to generate new hypotheses on the behavior of various molecular components in the NF-κB pathway [23–26]. However, information about spatial organization of these components, such as the oligomerization of TRAF proteins, has not been incorporated into these models. On the other hand, methods in another class of simulation technique, including MCELL [27], Smoldyn [28, 29] and more recently SpringSaLaD [30, 31], use lattice-based or particle-based models to implement the diffusions of biomolecules within a more realistic cellular environment. They can be used to simulate the formation of spatial patterns on the subcellular level, such as protein complex assembly or phase separation [32–40]. Unfortunately, these methods are intractable to be applied to study the dynamics of an entire signaling pathway because of their high demands for computational resources. Overall, it is highly challenging to develop a simulation method, which is able to capture a signaling event with both spatial resolution and its functional impacts on the whole signaling networks.

In order to overcome this challenge, a hybrid simulation approach is presented to describe the dynamics in the NF-κB signaling pathway. The method contains two coupled systems. The assembly of TRAF-based signaling platform at the membrane proximal region is modeled by a rigid body-based diffusion–reaction algorithm, whereas the downstream signaling events, including the recruitment of IκB kinase (IKK), phosphorylation of IκB and activation of NF-κB, are simulated as stochastic chemical reactions. These two levels of simulations are integrated together, so that how spatial variations in the signaling platform affect the rest of the pathway can be quantitatively analyzed. The signaling network is further regulated by negative feedbacks through different inhibitors such as IκB and A_{20}, which leads to an oscillatory NF-κB response. We demonstrated that the temporal patterns of downstream signal oscillations are closely correlated with the spatial organization of upstream platform assembly. Our simulation results also suggested that the cellular dynamics of NF-κB signaling pathway can be fine-tuned by a single pair of molecular interaction between TRAF proteins. Altogether, this study sheds light on the basic mechanism of NF-κB signaling pathway and highlights the functional importance of spatial regulation. The hybrid simulation framework also showcases its potential of application to other systems of cell signaling pathways.

RESULTS AND DISCUSSIONS

General description of the outputs from simulations of the signaling network

Most members in TRAF family contain a RING domain at their N-terminus, a TRAF-C domain at their C-terminus and a coiled-coil region in the middle [41]. Although the C-terminal domain of TRAF maintains interactions with upstream receptors, the N-terminal regions function as platform to mediate the downstream poly-ubiquitination, as well as the *cis*-interactions between themselves [18]. Moreover, most members in TRAF family form trimeric quaternary structure through their coiled-coil regions [42]. We are mainly focusing on the spatial clustering of TRAF trimers and its impacts on regulating the downstream signaling dynamics. The formation of upstream ligand–receptor complex is beyond the scope of this study. As a result, we assume that the ligand–receptor complexes have already preformed on cell surface before our simulations and the trimeric scaffold proteins have already bound to the cytoplasmic domains of receptors (Fig. 1a). Based on this assumption, the TRAF trimer and the ligand–receptor complex are modeled as one single rigid body attached to the cell membrane. Each rigid body contains three binding sites to maintain the *cis*-interaction between TRAF trimers. The movements of each TRAF trimer are confined within the 2D membrane proximal area. The multiple *cis*-interactions involved in each TRAF trimer and its 2D movements can further result in the higher-order clustering, which is simulated by a diffusion–reaction algorithm. Detailed model representation of TRAF trimers and the follow-up algorithm used to simulate their clustering are described in the Methods.

The formation of a *cis*-interaction between two TRAF trimers further facilitates the assembly of linear ubiquitin chain assembly complex (LUBAC) [43]. The LUBAC further provides the scaffold to enable the activation of the kinases IKK. Upon activation, IKK can induce the phosphorylation of IκB, which forms a complex with the transcription factor NF-κB as an inhibitor

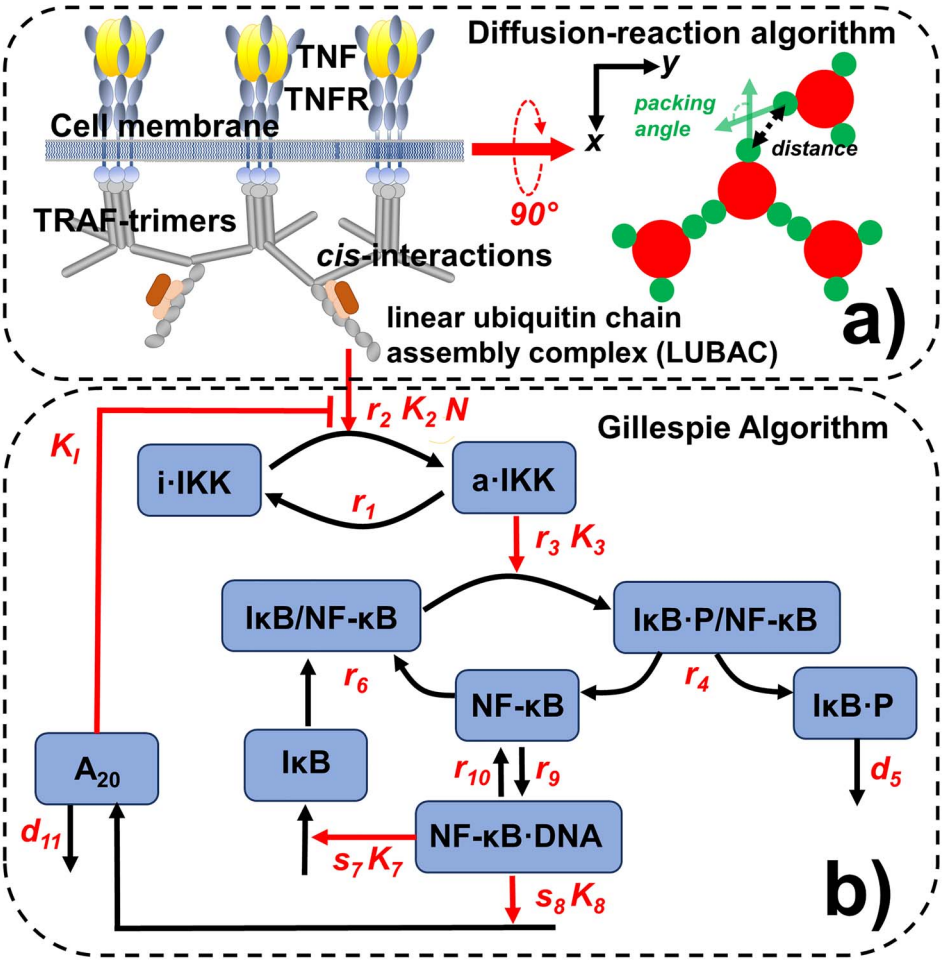

Figure 1. The dynamics of the NF-κB signaling pathway is simulated by a computational method consisting of two coupled systems. The assembly of TRAF-based signaling platform at the membrane proximal region is modeled by a rigid body-based diffusion–reaction algorithm, as shown in (a). We assume that each TRAF trimer has bound to its upstream ligand–receptor complex and therefore is modeled as a single rigid body, in which movements are confined within the 2D membrane proximal area. The formation of a *cis*-interaction between two TRAF trimers thus facilitates the assembly of linear ubiquitin chain assembly complex (LUBAC). The LUBAC further provide the scaffold to enable the activation of downstream signaling pathway, for which diagram is sketched in (b). The dynamics of the signaling network are simulated by Gillespie algorithm. Finally, the diffusion–reaction and Gillespie algorithms are synchronized under a multiscale simulation framework, as described in the Methods.

[11]. The complex will be dissociated after the phosphorylation of IκB, so that the transcription factor can be freely released. The phosphorylated inhibitor later undergoes ubiquitin-dependent proteolysis, whereas the released transcription factor enters cell nucleus and bind to the promoter and turn on its target genes. The genetic regulation of two proteins is specific modeled in the network. The first is the inhibitor IκB itself. The newly synthesized IκB enters cytoplasm and associates with free NF-κB to block its function as a transcription regulator [44]. The second protein in which gene is also turned on by NF-κB is A_{20}. Upon synthesis, the protein also functions as an inhibitor to diminish the activation process of IKK [45]. The diagram of the network is shown in Fig. 1b, whereas its mathematical description is presented in the Method.

Based on the mathematical representation of all reactions in the signaling network, the dynamics of the system is simulated stochastically by Gillespie algorithm. The signaling network has further been coupled with the spatial clustering of TRAF trimers under a hybrid simulation framework. The specific procedure of the hybrid simulation, which combined Gillespie algorithm with the spatial model of TRAF clustering, is delineated in the Method. The results from this hybrid simulation are summarized in Fig. 2. Specifically, 200 TRAF trimers were randomly placed in the 2D membrane proximal region as an initial configuration (Fig. 2a). The length of each side in this square region is 1000 nm, along both *X* and Y directions, which gives a total area of 1 μm^2. Some representative snapshots of the clustering process are also plotted along the simulation trajectory. We found that TRAF trimers start to aggregate into small oligomers (Fig. 2b). These oligomers are organized into hexagonal lattice based on the spatial symmetry of three binding sites in each trimer. The formation of these oligomers is a very dynamic process. TRAF trimers constantly left one oligomer and joined another one. As a result, small oligomers either disappeared or merged into neighboring larger oligomers, leading into a configuration in which the number of clusters became smaller and their sizes continued growing, as shown in Fig. 2c. Ultimately, most trimers aggregated together into a final larger cluster and the system reached equilibrium, as shown in Fig. 2d.

The number of *cis*-interactions formed between TRAF trimers was further plotted in Fig. 2e as a function of simulation time steps. The figure shows that the number of *cis*-interactions

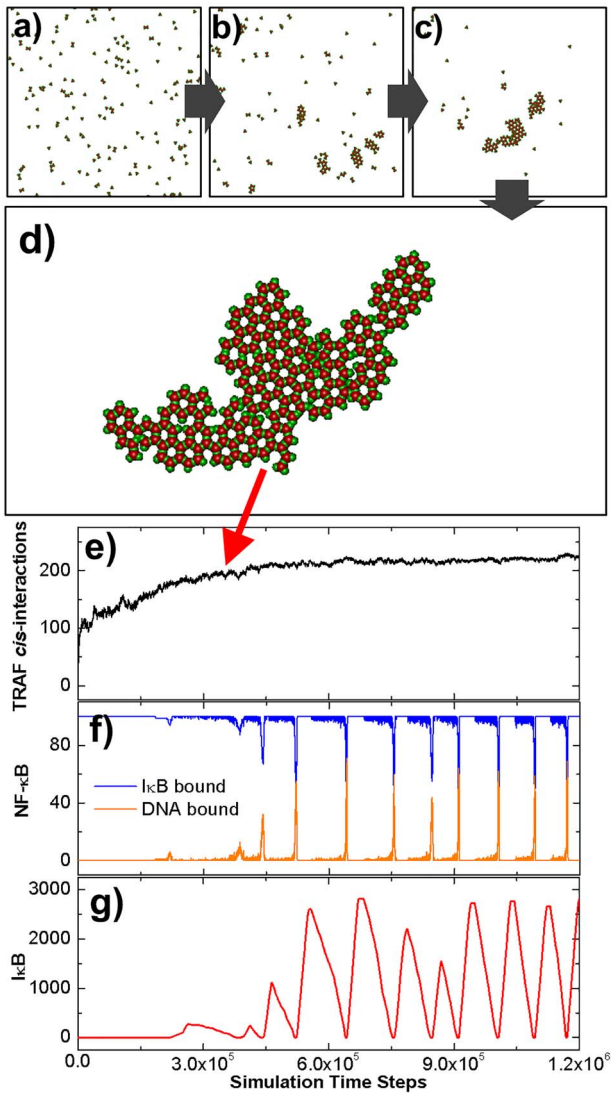

Figure 2. The initial configuration of the diffusion–reaction simulation is shown in (a). Some representative snapshots along the simulation trajectory were selected in (b) and (c). The configuration that the system reached equilibrium is further shown in (d). In (e), we plotted the number of *cis*-interactions between TRAF trimers observed in the system along with the simulation time steps. The kinetic profiles of molecular components in the downstream signaling network were further plotted as functions of simulation time steps. These profiles are the numbers of NF-κB molecules, which bind to IκB and DNA, as shown by the blue and orange curves in (f), and the total number of free IκB in the system, as shown by the red curve in (g).

increased very fast at the beginning of the simulation, indicating an initial seeding process. The increase of *cis*-interactions became slower as the oligomers in the system grew, and finally reached saturation after 4.5×10^5 simulation time steps, corresponding to the formation of the final cluster. The kinetic profiles of molecules in the downstream signaling network were further plotted in the following figures. Specifically, the numbers of NF-κB molecules, which bind to IκB and DNA, are shown in blue and orange curves in Fig. 2f, respectively. A periodic boost of DNA-bound NF-κB is displayed in the figure, corresponding to the timing of dissociation between NF-κB and IκB. Following the cycle of NF-κB, the total number of free IκB in the system also oscillated along the simulation, as illustrated in Fig. 2g. This oscillatory behavior is the result of the negative feedback regulation in the network, which is implemented by IκB and A_{20}. In addition, we found that the oscillation was initiated after the number of total *cis*-interactions between TRAF trimers almost stop changing, indicating that the formation of large clusters is critical to activate the downstream signaling pathway. In summary, our simulation results showcased the oscillatory dynamics in the NF-κB signaling pathway and its correlation with the spatial organization of molecular components in the pathway.

The comparison of signaling dynamics in systems with and without TRAF clustering

In order to further elucidate the functional importance of TRAF clustering in regulation of downstream signaling pathway, we carried out two separate simulations with different scenarios. The TRAF trimers in the first scenario, as we descried before, contain three binding sites. As a result, each trimer can simultaneously form *cis*-interactions with three structural neighbors, leading into the formation of a highly ordered spatial pattern. In contrast, a control system was designed in the second scenario. In this control system, we disabled the possibility of high-order clustering among TRAF proteins. This was achieved by assigning only one binding site to each TRAF protein instead of three, so that only *cis*-dimers can be formed between two proteins. As the initial configuration of the first scenario, 200 rigid bodies of TRAF trimers were randomly placed on a 2D square surface with an area of 1000×1000 nm^2. On the other hand, the control simulation contains 600 rigid bodies randomly distributed on the surface with the same area to maintain the same level of possible total interactions as in the first scenario. All the other parameters in the diffusion–reaction simulation of control scenario such as diffusion and binding constants remain unchanged. The binding affinity of *cis*-interactions in both systems equals −10 kT. Moreover, in the stochastic simulations of downstream signaling network, the same values of rate constants were used for the second scenario as for the first scenario.

The comparison of simulation results between these two scenarios is summarized in Fig. 3. The total number of *cis*-interactions formed between TRAF trimers along the simulation in the first system is plotted by the red curve in Fig. 3a, whereas the total number of dimerized *cis*-interactions formed in the control system is plotted by the red curve. The figure shows that the number of *cis*-interactions in the system, which can form clusters, grew more slowly, but reached a much higher level than the system, which can only form dimers, although the binding affinity and total binding sites in both systems are the same. Moreover, the level of fluctuations in the first system is also lower than the second one. The final configurations at the end of two simulations are compared with each other in Fig. 3c and d, respectively. Different from a small number of large clusters oligomerized in the first system, a large number of dimers are randomly distributed in the control system.

In order to quantitatively estimate the statistical significance of observed differences between these two systems, a two-sample student's *t*-test was carried out to the data collected from these two trajectories, in which distributions are plotted as histograms in Fig. 3b. In detail, the average number of *cis*-interactions in the distribution of dimerized system is 75.51 and its standard deviation equals 7.16. Relatively, the average number of *cis*-interactions in the distribution of oligomerized system is 182.53 and its standard deviation equals 3.04. The null

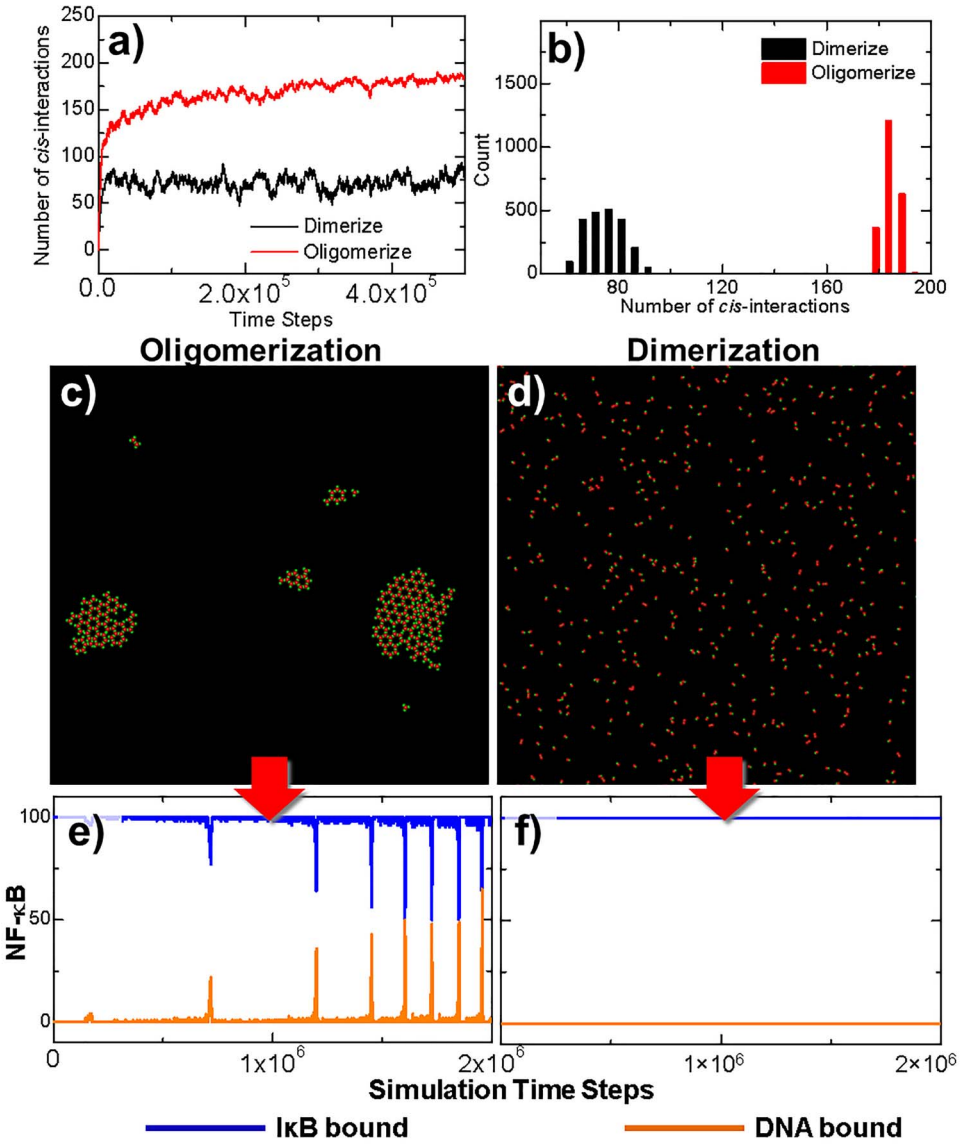

Figure 3. Two simulation scenarios were designed to elucidate the functional importance of TRAF clustering in regulation of downstream signaling pathway. The TRAF trimers in the first scenario contain three binding sites and can simultaneously form *cis*-interactions with three structural neighbors, whereas in a control system, only one binding site was assigned to each TRAF protein. The numbers of *cis*-interactions formed along the simulations in these two scenarios are plotted in (a). The distributions of fluctuations in the number of *cis*-interactions are shown as histograms in (b). The final configurations at the end of two simulation systems are compared with each other in (c) and (d). Finally, the outputs from the downstream signaling networks of these two systems, e.g. the numbers of NF-κB molecules, which bind to IκB and DNA, are also compared with each other in (e) and (f), respectively.

hypothesis is that no difference exists between two distributions. It was tested at a 95% confidence interval. The calculated *t*-score equals 650.28 with the *P* value <0.0001. This small *P* value from the *t*-test indicates that the null hypothesis can be rejected and the alternative hypothesis can be accepted, i.e. the spatial arrangement of TRAF oligomers lead into significant change in the level of *cis*-interactions comparing with the system in which oligomers are not allowed to form.

The outputs from the downstream signaling networks of the two comparative systems are shown in the following panels of the figure. The changes of NF-κB that bound to IκB or DNA in the first system are plotted as a function of the simulation time with blue and yellow curves in Fig. 3e. The oscillations were observed in the system, in which the number of NF-κB/DNA complexes was boosted periodically after the clusters of TRAF trimers were stabilized, corresponding to the red curve in Fig. 3a. The impulse of NF-κB/DNA complexes is coincident with the drop of NF-κB/IκB complexes, which is due to the phosphorylation of IκB by activated IKK. This oscillatory dynamic of components in the network indicates that the signaling pathway was turned on by the clustering of TRAF trimers. In contrast, the number of NF-κB/IκB complexes remained at its initial level throughout the simulation in the second system. As a result, no NF-κB/DNA complex was obtained before the end of the simulation, corresponding to the curves plotted in Fig. 3f. This result suggests that the signaling pathway could not be effectively turned on due to the less numbers and higher fluctuations of *cis*-dimers formed in the control scenario.

In summary, this comparative study demonstrated the possibility that systems with the same sets of rate parameters can evolve into very different temporal dynamics, only because of the different spatial organizations of signaling molecules. More specifically, a threshold-like behavior is controlled by the geometric arrangement of *cis*-interaction between TRAF scaffold proteins. Multiple binding sites in TRAF trimers lead to their high-order aggregation at membrane proximal region. Comparing with the regular dimer, each trimer in a cluster is simultaneously involved in three *cis*-interactions with its neighbor. These interlocked systems are kinetically more difficult to be dissociated. Consequently, they provide stable platform to downstream signal activation. Without this trimeric quaternary structure, on the other hand, TRAF proteins can only dimerize. Comparing with the highly ordered oligomers, these dimers are easier to be dissociated, although the binding affinity of the *cis*-interaction remains unchanged. As a result, the poly-ubiquitination facilitated by dimerized TRAF proteins alone cannot pass the threshold of downstream signal activation.

Change in the binding constants in the oligomerization

We have estimated the importance of TRAF trimers' multiple *cis*-binding sites not only in their assembly into higher-order structures, but also in the initiation of NF-κB signaling pathway. In this section, we further explore the energetic impacts of this *cis*-interaction on spatial–temporal dynamics of the system. Specifically, the binding affinity for a given pair of binding sites between two TRAF trimers was charged to different values in the diffusion–reaction simulation. Three scenarios were tested separately. A weak binding affinity (-6 kT) was used in the first scenario. In comparison, a strong binding affinity (-14 kT) was used in the second scenario. In addition to these two systems, a moderate value of binding affinity (-8 kT) was also tested as the third scenario. All the other parameters in both TRAF clustering section and signaling network section of the simulations are the same. The kinetic profiles generated from the simulations of these three systems are plotted in Fig. 4.

The numbers of *cis*-interactions formed in the three scenarios are plotted in Fig. 4a as a function of simulation time steps. The profile with the weak binding affinity is shown by the black curve, which indicates a low number of *cis*-interactions. On the other hand, a much higher level of *cis*-interactions were derived in the system with strong binding affinity, as shown by the blue curve. A more interesting kinetic profile was observed in the system with moderate binding affinity, corresponding to the red curve in Fig. 4a. The figure suggests that a small reduce of affinity from -6 to -8 kT significantly increased the level of *cis*-interactions. Surprisingly, the number of total interactions formed by the end of the simulation with moderate binding affinity is >200, even higher than the number found in the system with much stronger *cis*-interactions. Moreover, comparing with the system of strong affinity, which reached equilibrium at the very early stage of simulation, the number of *cis*-interactions in the system of moderate binding affinity increased much slower.

The dynamics in the downstream signaling networks of three systems are further shown in Fig. 4b. The changes of free IκB are plotted as a function of simulation time steps. An oscillation on the level of IκB was observed in the system of moderate binding affinity, as shown by the red curve in the figure. The oscillation was started when the stimulation time reached 1×10^5 steps, consistent with the stage as the number of *cis*-interactions in the system did not further increase (shown by the red curve in Fig. 4a). In contrast, no free IκB was observed in the system with weak binding affinity. This is due to the low level of *cis*-interactions formed in the system. The poly-ubiquitin chains recruited by this small number of *cis*-interaction between TRAF proteins were not enough to active IKK in the system and prevented the IκB from being phosphorylated. As a result, the genes regulated by NF-κB cannot be turned on throughout the simulation. It is worth mentioning that no oscillation of free IκB was also obtained in the system with strong binding affinity. The IκB was produced at very late stage of the simulation after the time passed 4×10^5 steps. However, it reached to a very low level, but then start to decay all the way through the end of the simulation, as shown by the blue curve in Fig. 4b. The results from the simulations of these three systems therefore suggest that the oscillatory patterns of the signaling dynamics are very sensitive to the strength of *cis*-interaction between TRAF proteins.

In order to test the correlation between the oscillatory patterns of the signaling pathway and the binding affinity of the *cis*-interaction on a more statistically meaningful level, systematical tests were carried out to systems in which binding affinities of *cis*-interaction were ranged from -6 to -15 kT, with an interval of 1 kT. Multiple trajectories were generated for each system, while a longer simulation time (2×10^6 steps) was given for each trajectory. At the end of all simulations, we counted the number of oscillatory periods observed in each trajectory. The average number of oscillatory periods was then calculated for each system depending on the values of binding affinity. The calculated results are summarized in Fig. 4c as striped bars in the histogram. The figure confirms that oscillations were not observed under weak binding affinities, but suddenly appeared when affinities are below -7 kT, suggesting that there is phase transition in the system. Further enhancement of binding affinity does not change the frequency of oscillation too much until it becomes stronger than -12 kT. Above this region, the oscillatory frequency will be gradually reduced if the *cis*-binding affinity increases. Finally, no more oscillation exists after the binding affinity equals -15 kT. This is consistent with the signaling outputs illustrated in Fig. 4b.

In parallel, the same systematical tests were carried out to the control systems. Specifically, binding affinities of *cis*-interaction were also assigned from -6 to -15 kT, with an interval of 1 kT. The same values were applied to all the other simulation parameters, except that only *cis*-dimers can be formed between two TRAF proteins in the control system. After all simulations are completed, we calculated the average number of oscillatory periods for different testing values of binding affinity. The calculated results are shown by black bars in the histogram of Fig. 4c. In contrast to the oligomerization system, oscillations can only be observed in the dimerization system when the binding affinity of *cis*-interactions is stronger than -13 kT. The comparison of these two systems thus highlights the functions of TRAF oligomerization in regulating the downstream signaling as follows. First, signaling can solely be activated by the oligomerization of TRAF proteins if the binding affinity of their *cis*-interactions is in the moderate range between -8 and -13 kT. If the binding affinity becomes stronger, oscillation can be activated without oligomerization due to the increasing number of *cis*-interactions formed in the system. Interestingly, our simulation results suggest that oligomerization under these strong *cis*-interactions will inhibit downstream signaling. As described later, the inhibition was achieved by kinetically segregating TRAF trimers in small clusters. This provides a potential mechanism to suppress the original signaling. Therefore, our study demonstrated that the dynamic outcome of a signaling network can be

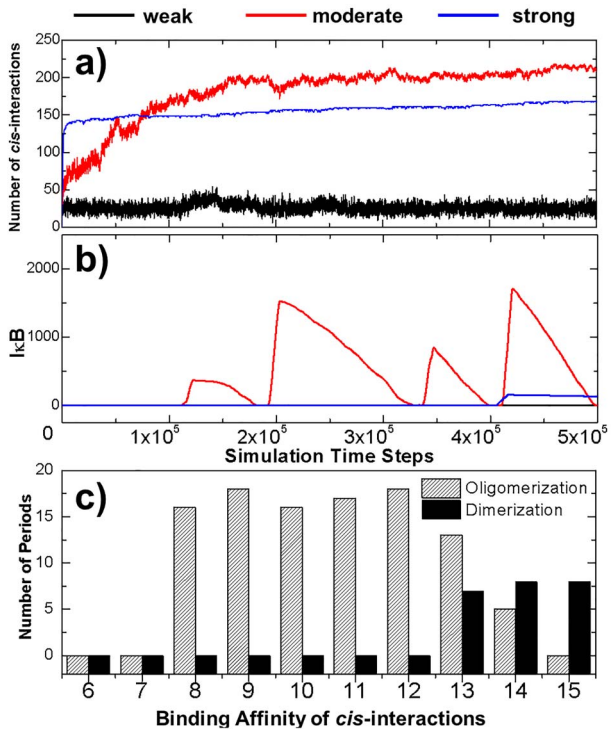

Figure 4. In order to explore the energetic impacts of the *cis*-interaction between TRAF trimers on spatial–temporal dynamics of the system, three scenarios with the weak-, moderate- and strong-binding affinities of these *cis*-interactions were tested separately. The numbers of *cis*-interactions formed in these three scenarios are plotted in (a) as a function of simulation time steps, whereas the numbers of free IκB in the system are shown in (b). More systematical tests were further carried out, in which we changed the binding affinities of *cis*-interaction from −6 to −15 kT, with an interval of 1 kT for both dimerization and oligomerization systems. The average numbers of oscillation periods were derived from the multiple trajectories of these systems and were plotted as histogram in (c) as a function of *cis*-binding affinity. The results from the oligomerization system are shown by the striped bars, whereas the results from the dimerization control system are shown by the black bars.

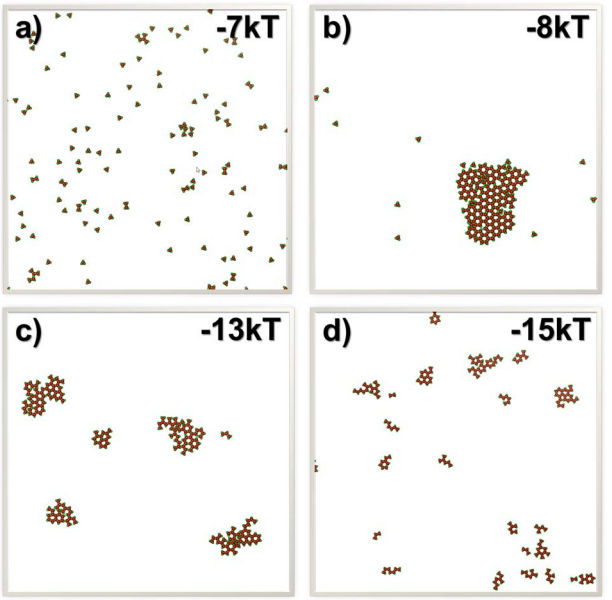

Figure 5. To illustrate the relation between the spatial properties of TRAF clusters and the strength of their *cis*-interactions, the final configurations from the systems in which binding affinities equal −7 and −8 kT are plotted in (a) and (b). These two plots show that the clustering can generate very different spatial pattern with only a slight change in the binding affinity. On the other hand, the final configurations from the systems in which binding affinities equal −13 and −15 kT are plotted in (c) and (d), respectively. These two plots suggest that systems with stronger binding affinity contain more clusters with smaller sizes.

modified either positively or negatively by the spatial organization of protein–protein interactions in the system, depending on the strength of their binding affinity.

Unfortunately, there is no experimentally measured binding affinity available in the literatures for the *cis*-interaction between TRAF trimers. The only experimental data is the dimerization in the crystal structure of TRAF6 through their N-terminal RING and zinc finger domains [16]. The crystal structure (PDB ID 3HCS) shows the binding interface buries a total of 1270 Å^2 surface areas. Furthermore, most intermolecular interactions in the binding areas are hydrophobic, but not electrostatic interactions, which could lead to stronger binding. Using the size of buried surface areas and their hydrophobic nature, we estimate that the dissociation constant of *cis*-interactions between TRA6 is within a moderate range from millimolar to micromolar, which corresponds to the binding affinity between −9 and −13 kT. This estimation is based on a previous statistical analysis of correlation between buried surface areas and experimentally measured dissociation constants for 113 protein complexes [46]. As shown above, within this range of binding affinity, the oscillation of NF-κB signals can only be activated through the spatial oligomerization of TRAF trimers. Finally, it is worth mentioning that this is just an insight only for TRAF6. Binding affinities could variate among members in the TRAF family. Also, the real binding between TRAF in cellular environments could also be very different from the *in vitro* measurements.

To further understand how NF-κB signals can be spatially regulated by TRAF protein clustering, the final configurations from some of the simulation systems were plotted in Fig. 5. The final configurations from the systems in which binding affinities equal −7 and −8 kT are shown in Fig. 5a and b, respectively. With only a slight change in the binding affinity, very different spatial pattern was derived in the figures. This difference can be explained by the phase transition of TRAF clustering, which drives the system from a scattered distribution of trimers to their condensation into a single cluster. The network of trimers formed within the cluster stabilizes the *cis*-interactions and thus facilitate the signal activation of downstream pathway. In comparison, the final configurations from two systems selected from the other end of the binding affinity are shown in Fig. 5c and d. These figures show that systems with stronger binding affinity contain more clusters with smaller sizes. Comparing with the signal big cluster formed in the system with binding affinity of −8 kT, five clusters were obtained in the system with binding affinity of −13 kT and each cluster on average contains 40 trimers, as shown in Fig. 5c. When the binding affinity reaches −15 kT, as shown in Fig. 5d, the number of clusters in the system increases to 20 and each cluster on average only contains 10 TRAF trimers. These results suggest that the strong binding affinities kinetically trap TRAF trimers into small clusters, which plays negative role in activating the oscillations in the downstream signaling network.

More specifically, the formation of a single larger cluster is resulted from the competition among different oligomers, in which TRAF trimers constantly leave one oligomer and join another. Through this dynamic process, oligomers with

Table 1. The information about the simulation parameters in the signaling network.

Index	Description	Mathematical representation	Parameter	Value	Remark
1	Deactivation of IKK	$r_1[a \cdot \mathrm{IKK(t)}]$	r_1	0.2 s^{-1}	Rate of transition
2	Activation of IKK	$r_2[\mathrm{i} \cdot \mathrm{IKK(t)}] \times \frac{[\mathrm{LUBAC(t)}]^N}{[\mathrm{LUBAC(t)}]^N + [K_2 \times (1 + [\mathrm{A_{20}(t)}]/K_I)]^N}$	r_2	0.4 s^{-1}	Maximal rate of catalysis
			K_2	240 nM	Saturation coefficient of catalysis
			K_I	10 nM	Inhibition coefficient of catalysis
			N	25	Hill coefficient
3	Phosphorylation of IκB	$\frac{r_3[a \cdot \mathrm{IKK(t)}][\mathrm{I\kappa B/NF\text{-}\kappa B(t)}]}{[\mathrm{I\kappa B/NF\text{-}\kappa B(t)}] + K_3}$	r_3	0.08 s^{-1}	Maximal rate of catalysis
			K_3	500 nM	Saturation coefficient of catalysis
4	Dissociation of IκB/NF-κB complex	$r_4[\mathrm{I\kappa B} \cdot \mathrm{P/NF\text{-}\kappa B(t)}]$	r_4	0.4 s^{-1}	Dissociation rate
5	Degradation of IκB	d_5	d_5	0.8 nMs^{-1}	Degradation rate
6	Association of IκB/NF-κB complex	$r_6[\mathrm{I\kappa B(t)}][\mathrm{NF\text{-}\kappa B(t)}]$	r_6	0.008 $nM^{-1}s^{-1}$	Association rate
7	Synthesis of IκB	$\frac{s_7[\mathrm{NF\text{-}\kappa B \cdot DNA(t-\tau)}]}{[\mathrm{NF\text{-}\kappa B \cdot DNA(t-\tau)}] + K_7}$	s_7	0.8 s^{-1}	Maximal rate of synthesis
			K_7	50 nM	Saturation coefficient of synthesis
8	Synthesis of A_{20}	$\frac{s_8[NF-\kappa B \cdot DNA(t-\tau)]}{[NF-\kappa B \cdot DNA(t-\tau)] + K_8}$	s_8	0.4 s^{-1}	Maximal rate of synthesis
			K_8	100 nM	Saturation coefficient of synthesis
9	Association of NF-κB with DNA	$r_9[\mathrm{NF\text{-}\kappa B(t)}]$	r_9	0.8 s^{-1}	Transition rate
10	Dissociation of NF-κB from DNA	$r_{10}[\mathrm{NF\text{-}\kappa B} \cdot \mathrm{DNA(t)}]$	r_{10}	0.08 s^{-1}	Transition rate
11	Degradation of A_{20}	d_{11}	d_{11}	0.1 nMs^{-1}	Degradation rate

smaller sizes gradually dissolve or merge into neighboring oligomers. Meanwhile, TRAF trimers join and are then stabilized by oligomers with larger sizes, leading into their continuous growth. Protein complexes are difficult to dissociate into monomers under strong binding affinities, whereas the multivalency of TRAF trimers makes dissociation much more difficult after they were initially captured by an oligomer. Consequently, these small oligomers are maintained throughout the simulations. It is worth mentioning that the segregation of TRAF trimers into small oligomers under strong binding affinity is only a kinetic phenomenon within our limited simulation timescale. Thermodynamically, the system still prefers the formation of a single larger cluster. As reflected by the blue curve in Fig. 4b, although extremely slow, the number of *cis*-interactions under strong binding affinity still keeps increasing until the end of the simulation. Therefore, we believe that the system will ultimately reach equilibrium by forming a large cluster by the time the oscillations will be activated. However, this process is beyond the timescale that our computational simulation can observe. It might also be beyond the real timescale required for cell signaling pathways and becomes less biologically meaningful.

Taken together, our simulation results show that the increase of *cis*-binding affinity triggers the phase transition of TRAF clustering. This phase transition results in a threshold-like signal response from the downstream pathway. Moreover, the large-scale TRAF clusters is kinetically slow to assemble, but highly stable after its formation. This slow kinetics of the assembling process and high stability of the clustered structure assure that the signaling pathway only response to a persistent and high dose of extracellular stimulations, and, therefore, promote the fidelity of signal transduction within stochastic cellular environments [47]. Finally, the oscillation of NF-κB signals can only be archived through a very dynamic process by *cis*-interactions with moderate binding affinities. The TRAF proteins with overly strong *cis*-interactions will be kinetically trapped in small clusters, and further impede their function in activating the downstream signal oscillation. This suggests that the molecular interactions in the NF-κB signaling pathway are tuned within a specific range by natural selection to maintain its appropriate functions.

CONCLUSIONS

NF-κB signaling pathway is one of the most important cell signaling pathways involved in inflammatory responses [48]. Recent experimental evidences started to show that signal transduction in the pathway is spatially modulated by its different molecular components [49]. However, the molecular mechanism of these spatial regulation and their functional impacts are not well understood. In order to tackle this problem, we developed a hybrid model in which the NF-κB signaling pathway is decomposed into two simulation scenarios. The physical process of TRAF clustering at membrane proximal region is simulated by a rigid body-based diffusion–reaction algorithm, whereas the downstream signaling network is simulated by stochastic simulation with Gillespie algorithm. These two algorithms are further synchronized under a multiscale simulation framework. Using this simulation method, we illustrated that the formation of TRAF-mediated 2D signaling platform is a critical factor to regulate the downstream oscillatory dynamics in the signaling network. The modification of *cis*-interaction between TRAF proteins leads to the changes of their clustering patterns

at membrane proximal regions, and further affects the NF-κB response. Interestingly, our results show that mutations either weaken or strengthen this *cis*-interaction and can cause the abolishment of oscillation in the pathway. This observation suggests that molecular elements and their interactions in a signaling network are elaborately designed to carry out their appropriate functions. In summary, the hybrid simulation developed in this study shows possibility to model a signaling system with both spatial resolution and functional implication. The results from the simulations provides the general biological insights to the interplay between the spatial assembly of individual signaling molecules and the threshold-like output from the entire signaling network, which offers a potentially new way to control signaling pathways in cellular systems.

METHODS

Mathematical representation of the signaling network

Following the spatial assembly of TRAF signaling platform, the changes of population for each type of molecular components in the downstream signaling network are quantitatively described by a set of ODE. Specifically, the numbers of active IKK and inactive IKK in the system at time t are changed by solving the following two equations:

$$\frac{d\left[a\cdot \mathrm{IKK}(t)\right]}{dt} = -r_1\left[a\cdot \mathrm{IKK}(t)\right] + r_2\left[\mathrm{i}\cdot \mathrm{IKK}(t)\right] \times \frac{\left[\mathrm{LUBAC}(t)\right]^N}{\left[\mathrm{LUBAC}(t)\right]^N + \left[K_2\times\left(1+\left[\mathrm{A}_{20}(t)\right]/K_I\right)\right]^N} \quad (1)$$

$$\frac{d\left[\mathrm{i}\cdot \mathrm{IKK}(t)\right]}{dt} = r_1\left[a\cdot \mathrm{IKK}(t)\right] - r_2\left[\mathrm{i}\cdot \mathrm{IKK}(t)\right] \times \frac{\left[\mathrm{LUBAC}(t)\right]^N}{\left[\mathrm{LUBAC}(t)\right]^N + \left[K_2\times\left(1+\left[\mathrm{A}_{20}(t)\right]/K_I\right)\right]^N} \quad (2)$$

In above equations, [a·IKK(t)] and [i·IKK(t)] are the numbers of active IKK and inactive IKK at time t, respectively. The first term on the right-hand side of equation (1) represents the transition of IKK from its active form to inactive form, where the parameter r_1 indicates the rate of the transition. The second term on the right-hand side of equation (1) represents the transition of IKK from its inactive form to active form. This reaction is catalyzed by the upstream poly-ubiquitin chains LUBAC, in which r_2 and K_2 are the maximal rate and saturation coefficient in the catalysis. The number of poly-ubiquitin chains in the system [LUBAC(t)] is determined by the number of *cis*-interactions between TRAF trimers in the upstream signaling platform. After forming *cis*-interactions, it has also been observed that the N-terminal RING domain of TRAF6 functions as an E3 ubiquitin ligase. It recruits the E2 ubiquitin-conjugating enzyme such as Ubc13 so that the poly-ubiquitin chains can be formed, leading into the assembly of LUBAC [50]. Therefore, in current study, the number of *cis*-interactions between TRAF trimers in the upstream signaling platform and the number of polyubiquitin chains in the system [LUBAC(t)] have a one-to-one relationship. Ideally, the LUBAC assembly could be modeled by an extra reaction as $[cis-\mathrm{interaction}(t)] \rightarrow [\mathrm{LUBAC}(t)]$, because it takes a non-zero amount of time to form these poly-ubiquitin chains once *cis*-interactions are formed. In order to minimize the complexity of our system, this first-order reaction was not incorporated into the model. We assume that this additional step would not affect the global dynamics of the signaling network and thus change the conclusions of our study.

Considering that LUBAC itself is a highly ordered signaling machinery, a Hill coefficient [51] N is further used to model the cooperativity in its assembly and its recruitment of IKK. Finally, the catalysis of this transition reaction is also restrained by protein A_{20} as a competitive inhibitor. The efficiency of inhibition is controlled by the concentration of A_{20} and the parameter K_I.

The activated IKK kinase further phosphorylates the inhibitory IκB subunit in the IκB/NF-κB complex. The number of phosphorylated complexes in the system at time t can be changed by solving the following equation:

$$\frac{d\left[\mathrm{I\kappa B}\cdot \mathrm{P/NF\text{-}\kappa B}(t)\right]}{dt} = -r_4\left[\mathrm{I\kappa B}\cdot \mathrm{P/NF\text{-}\kappa B}(t)\right] + \frac{r_3\left[a\cdot \mathrm{IKK}(t)\right]\left[\mathrm{I\kappa B/NF\text{-}\kappa B}(t)\right]}{\left[\mathrm{I\kappa B/NF\text{-}\kappa B}(t)\right]+K_3} \quad (3)$$

In above equation, [IκB/NF-κB(t)] and [IκB·P/NF-κB(t)] are the numbers of phosphorylated and unphosphorylated complex at time t, respectively. The second term on the right-hand side of equation (3) describes the phosphorylation process, in which rate depends on the concentration of activated IKK [a·IKK(t)]. The parameters r_3 and K_3 in the reaction are the maximal rate and saturation coefficient in the phosphorylation, as described by Michaelis–Menten kinetics. The first term on the right-hand side of equation (3) describes the dissociation reaction of IκB/NF-κB complex due to the phosphorylation of IκB, in which r_4 represents the rate constant of dissociation.

On the other hand, the number of unphosphorylated complex in the system is decreased by the IKK-induced phosphorylation, but increased by the association reaction between monomeric IκB and NF-κB, as described by the following equation:

$$\frac{d\left[\mathrm{I\kappa B/NF\text{-}\kappa B}(t)\right]}{dt} = -\frac{r_3\left[a\cdot \mathrm{IKK}(t)\right]\left[\mathrm{I\kappa B/NF\text{-}\kappa B}(t)\right]}{\left[\mathrm{I\kappa B/NF\text{-}\kappa B}(t)\right]+K_3} + r_6\left[\mathrm{I\kappa B}(t)\right]\left[\mathrm{NF\text{-}\kappa B}(t)\right] \quad (4)$$

The parameter r_6 in equation (4) is defined as the rate constant, which regulates the association between monomeric IκB and NF-κB in cytoplasm. Their numbers at time t, [IκB(t)] and [NF-κB(t)] are changed by the following two equations:

$$\frac{d\left[\mathrm{I\kappa B}(t)\right]}{dt} = \frac{s_7\left[\mathrm{NF\text{-}\kappa B}\cdot \mathrm{DNA}\,(t-\tau)\right]}{\left[\mathrm{NF\text{-}\kappa B}\cdot \mathrm{DNA}\,(t-\tau)\right]+K_7} - r_6\left[\mathrm{I\kappa B}(t)\right]\left[\mathrm{NF\text{-}\kappa B}(t)\right] \quad (5)$$

$$\frac{d\left[\mathrm{NF\text{-}\kappa B}(t)\right]}{dt} = r_4\left[\mathrm{I\kappa B}\cdot \mathrm{P/NF\text{-}\kappa B}(t)\right] - r_6\left[\mathrm{I\kappa B}(t)\right]\left[\mathrm{NF\text{-}\kappa B}(t)\right] + r_{10}\left[\mathrm{NF\text{-}\kappa B}\cdot \mathrm{DNA}(t)\right] - r_9\left[\mathrm{NF\text{-}\kappa B}(t)\right] \quad (6)$$

The second term on the right-hand side of equation (5) delineates the dissociation of IκB/NF-κB complex, as described above. In addition, the dissociation of NF-κB from phosphorylated IκB enters cell nucleus and binds to its targeted DNA sequence as a transcription factor. The formation of NF-κB·DNA complex regulates the expression of specific genes, including its own inhibitor IκB, which corresponds to the first term on the right-hand side of equation (5). We introduced the constant τ in the reaction to describe the time delay between NF-κB·DNA formation and IκB expression. We assume that the expression rate of IκB depends on the concentration of activated transcriptional factors [NF-κB·DNA($t-\tau$)] and reaches a maximum value s_7. The parameter

K_7 is the saturation coefficient in the regulation of protein synthesis, as described by Michaelis–Menten kinetics. In equation (6), on the other hand, the first two terms on its right-hand side have been introduced above, whereas the next two terms described the dynamic process in which NF-κB is translocated from cytoplasm into cell nucleus and binds to its target gene. Correspondingly, the parameters r_9 and r_{10} indicate the rates for the association and dissociation of the NF-κB·DNA complex, respectively. Given these two rate constants, the number of the NF-κB·DNA complex in the system at time t can be changed by solving the following equation:

$$\frac{d\left[\text{NF-}\kappa\text{B}\cdot\text{DNA}(t)\right]}{dt} = r_9\left[\text{NF-}\kappa\text{B}(t)\right] - r_{10}\left[\text{NF-}\kappa\text{B}\cdot\text{DNA}(t)\right] \quad (7)$$

Although the NF-κB dissociated from the IκB·P/NF-κB complex can either bind to DNA or reassociate with unphosphorylated IκB, the phosphorylated IκB that is dissociated from the IκB·P/NF-κB complex will be degraded with a rate constant d_5, as described by the following equation:

$$\frac{d\left[\text{I}\kappa\text{B}\times\text{P}(t)\right]}{dt} = r_4\left[\text{I}\kappa\text{B}\cdot\text{P/NF-}\kappa\text{B}(t)\right] - d_5 \quad (8)$$

Finally, the change of protein A_{20} is defined by the following equation:

$$\frac{d\left[\text{A}_{20}(t)\right]}{dt} = \frac{s_8\left[\text{NF-}\kappa\text{B}\cdot\text{DNA}\,(t-\tau)\right]}{\left[\text{NF-}\kappa\text{B}\cdot\text{DNA}\,(t-\tau)\right]+\text{K}_8} - d_{11} \quad (9)$$

Similarly, its expression is regulated by the NF-κB·DNA complex, as represented by the first term on the right-hand side of equation (9). The same constant τ is introduced to describe the time delay between NF-κB·DNA formation and A_{20} expression. The parameters s_8 and K_8 in the catalysis of protein synthesis give the maximal rate and saturation coefficient of the reaction, as described by Michaelis–Menten kinetics. The second term on the right-hand side of the equation determines the degradation rate of A_{20}.

Numerical algorithm of the hybrid simulation

The dynamics of the signaling pathway is simulated by two coupled modules. The oligomerization of TRAF scaffold proteins is simulated by a diffusion–reaction algorithm, whereas the downstream signaling events are simulated by the Gillespie algorithm. In the diffusion–reaction algorithm, we assume that the TRAF trimers have bound to the upstream ligand–receptor complexes. Therefore, their movements are confined within the membrane proximal area, which is modeled by a layer of 2D flat surface. Each TRAF protein, together with its upper-bound ligand–receptor complex, is modeled as a single rigid body. In order to capture the basic structural information of the trimeric scaffold protein, the rigid body further contains four connecting groups. The three TRAF-C domains and coiled-coil regions are placed at the center, surrounded by three other groups representing their RING domains. The angle between every two surrounding groups is 120°. Each surrounding group also contains a binding site to mimic the *cis*-interaction between RING domains.

Given the model representation, the diffusion–reaction simulation is started from an initial configuration, in which a large number of TRAF rigid bodies are randomly distributed within the 2D membrane proximal region. The kinetic Monte Carlo algorithm was implemented to operate the simulation. Each time step Δt in the simulation is broken down into two scenarios [52]. During the first scenario, all TRAF trimers are chosen by random order to undergo diffusions within the 2D area. The rotations of each trimer are restricted along the surface normal, whereas the translational movements are confined in the plain. The periodic boundary condition is applied so that any trimer leaving the 2D simulation box will enter its opposite side. More specifically, for translational diffusion, each TRAF trimer moves along a randomly selected direction in the plain with a fixed length, Δx. The probability of this random movement, P_T, is calculated by $P_T = 4D_T\Delta t/\Delta x^2$, in which D_T is the 2D translational diffusion constant. For rotational diffusion, each TRAF trimer is randomly rotated along the surface normal within the maximal value of $D_{R\times}\Delta t$, in which D_R is the effective rotational diffusion constant. After diffusion, if the center-to-center distance between two TRAF trimers, based on their new position, is smaller than the sum of their radii, the movement will be rejected to avoid potential collisions in the system. The values of diffusion coefficients were adopted from our previous studies as follows [53, 54]. The translational diffusion constant of a TRAF trimer equals 5 $\mu m^2/s$, and its rotational coefficient equals 0.25° per ns. Moreover, for the computational simplicity, if more than two TRAF trimers form a *cis*-interaction, they will stop diffusing as an initial seed to facilitate further oligomerization.

Following the scenario of molecular diffusions, the binding kinetics of *cis*-interaction between TRAF trimers are simulation in the second scenario. The association between two TRAF trimers can be triggered if (1) the distance between any binding sites within these two trimers is below a predetermined cutoff and (2) their packing angle equals 180°, as shown in Fig. 1a. Previous experimental evidences showed that the N-terminal RING domain of TRAF proteins can be dimerized both in the crystal and in solution [16]. It was further proposed that this dimerization of TRAF trimers can lead into the formation of a 2D hexagonal lattice, in which two trimers maintain a 2-fold symmetry through their *cis*-interaction [55, 56]. Based on these experimental insights, we assume that the packing angle between two TRAF trimers needs to be 180°. If a *cis*-interaction is formed between two trimers, they will stop diffusing to facilitate further oligomerization. On the other hand, dissociation of a *cis*-interaction occurs with a probability that is determined by its binding affinity. After dissociation, two trimers can either reassociate as a geminate recombination if the distance and packing angle between any pair of their binding sites satisfy the association criteria, or diffuse farther away from each other. The new configuration is updated at the end of each simulation time step after both diffusion and reaction scenarios are sequentially performed. Finally, the iteration of above diffusion–reaction process will not be terminated until the dynamics of the simulated system reaches equilibrium.

The high-order clusters formed by TRAF scaffold proteins provide a platform to recruit the poly-ubiquitin chains. The downstream signaling processes activated by the poly-ubiquitination are modeled by non-spatial stochastic simulation algorithm. This algorithm was developed by Gillespie in order to study biochemical reactions [57]. Given the initial condition of a signaling network, the populations of each molecular species in the system are propagated in a digitalized and stochastic manner. In detail, within each simulation step, the rates for all reactions are sequentially calculated by the mathematical formulas described in the previous section of the method. A cumulative distribution function is generated by adding up

all these rates. A random number is used to select one of these reactions based on the cumulative distribution function. Populations for all species are then updated according to the selected reaction. The simulation moves forward iteratively by above procedure. This Gillespie algorithm has further been coupled with the diffusion–reaction model [58], so that the spatial information of TRAF clustering can be integrated into the downstream signaling processes. Specifically, after the diffusion–reaction simulation, the number of newly formed *cis*-interactions between TRAF trimers can be obtained. Based on current knowledge about the function of TRAF protein in NF-κB signaling pathway, we assume that poly-ubiquitin chains are recruited at each *cis*-binding interface of TRAF trimers. Therefore, the number of LUBAC will be simultaneously updated. This new number of LUBAC enters the next step of the Gillespie simulation to guide the activation of IKK. In turn, the outputs from the Gillespie simulation affect the diffusion–reaction simulation as follow. Based on the Gillespie algorithm, the time of the simulation system is moved forward by a specific time interval τ. Given this new time interval, n steps of the diffusion–reaction simulation are carried out to generate a new spatial configuration. The number n is calculated as $\tau/\Delta t$, in which Δt is the length of the diffusion–reaction simulation time step. This calculation is to ensure that the timescale between spatial processes of TRAF clustering and the downstream signaling pathway can be synchronized.

We described a generic framework of NF-κB signaling network in which some factors have not been simulated before. It is not realistic to derive consistent model parameters from various experimental measurements or previous computational models. As a result, the values of all parameters were chosen on a heuristic basis from the biologically meaningful range, so that the oscillatory nature of the pathway under a persistent ligand stimulation can be qualitatively reproduced within the timescale that is close to the experimental observation. The values of these parameters in the simulation are listed in the Table 1. The variations in these parameters will not significantly affect the general dynamic patterns of the system. It is more important to recognize how the spatial–temporal dynamics of the signaling system is quantitatively modified by a small perturbation in the parameters space.

AUTHORS' CONTRIBUTIONS

K.D. and Y.W. designed the research; K.D. performed the research; K.D. and Z.S. analyzed the data; K.D. and Y.W. wrote the paper.

ACKNOWLEDGMENT

Computational support was provided by Albert Einstein College of Medicine High Performance Computing Center.

FUNDING

This work was supported by the National Institutes of Health (Grant Numbers R01GM120238 and R01GM122804). The work is also partially supported by a start-up grant from Albert Einstein College of Medicine.

CONFLICT OF INTEREST

None declared.

DATA AVAILABILITY

Data sharing is not applicable to this article as no datasets were generated or analyzed during the current study.

AVAILABILITY AND IMPLEMENTATION

The computational program was implemented by FORTRAN77. All the data and source code are available by contacting the corresponding author.

REFERENCES

1. Gobert AP, Wilson KT, Martin C. Cellular responses to attaching and effacing bacteria: activation and implication of the innate immune system. *Arch Immunol Ther Exp (Warsz)* 2005;**53**:234–44.
2. Lacy P, Stow JL. Cytokine release from innate immune cells: association with diverse membrane trafficking pathways. *Blood* 2011;**118**:9–18.
3. Coussens LM, Werb Z. Inflammation and cancer. *Nature* 2002;**420**:860–7.
4. Courtois G, Gilmore TD. Mutations in the NF-kappaB signaling pathway: implications for human disease. *Oncogene* 2006;**25**:6831–43.
5. Kumar V, Sharma A. Neutrophils: Cinderella of innate immune system. *Int Immunopharmacol* 2010;**10**: 1325–34.
6. Gilmore TD. Introduction to NF-kappaB: players, pathways, perspectives. *Oncogene* 2006;**25**:6680–4.
7. Brasier AR. The NF-kappaB regulatory network. *Cardiovasc Toxicol* 2006;**6**:111–30.
8. Akira S, Takeda K. Toll-like receptor signalling. *Nat Rev Immunol* 2004;**4**:499–511.
9. Park HH. Structure of TRAF family: current understanding of receptor recognition. *Front Immunol* 2018;**9**: 1999.
10. Lamothe B, Besse A, Campos AD, et al. Site-specific Lys-63-linked tumor necrosis factor receptor-associated factor 6 auto-ubiquitination is a critical determinant of I kappa B kinase activation. *J Biol Chem* 2007;**282**: 4102–12.
11. Ghosh S, Baltimore D. Activation in vitro of NF-kappa B by phosphorylation of its inhibitor I kappa B. *Nature* 1990;**344**:678–82.
12. Sen R, Baltimore D. Inducibility of kappa immunoglobulin enhancer-binding protein Nf-kappa B by a posttranslational mechanism. *Cell* 1986;**47**:921–8.
13. Cebecauer M, Spitaler M, Serge A, et al. Signalling complexes and clusters: functional advantages and methodological hurdles. *J Cell Sci* 2010;**123**:309–20.
14. Hartman NC, Groves JT. Signaling clusters in the cell membrane. *Curr Opin Cell Biol* 2011;**23**:370–6.
15. Napetschnig J, Wu H. Molecular basis of NF-kappaB signaling. *Annu Rev Biophys* 2013;**42**:443–68.
16. Yin Q, Lin SC, Lamothe B, et al. E2 interaction and dimerization in the crystal structure of TRAF6. *Nat Struct Mol Biol* 2009;**16**:658–66.
17. O'Neill LA, Bowie AG. The family of five: TIR-domain-containing adaptors in Toll-like receptor signalling. *Nat Rev Immunol* 2007;**7**:353–64.
18. Xie P. TRAF molecules in cell signaling and in human diseases. *J Mol Signal* 2013;**8**:7.

19. Middleton AJ, Budhidarmo R, Das A, et al. The activity of TRAF RING homo- and heterodimers is regulated by zinc finger 1. *Nat Commun* 2017;**8**:1788.
20. Cheong R, Hoffmann A, Levchenko A. Understanding NF-kappaB signaling via mathematical modeling. *Mol Syst Biol* 2008;**4**:192.
21. Cheong R, Bergmann A, Werner SL, et al. Transient IkappaB kinase activity mediates temporal NF-kappaB dynamics in response to a wide range of tumor necrosis factor-alpha doses. *J Biol Chem* 2006;**281**:2945–50.
22. Hoffmann A, Levchenko A, Scott ML, et al. The IkappaB-NF-kappaB signaling module: temporal control and selective gene activation. *Science* 2002;**298**:1241–5.
23. Pogson M, Holcombe M, Smallwood R, et al. Introducing spatial information into predictive NF-kappaB modelling–an agent-based approach. *PLoS One* 2008;**3**:e2367.
24. Pogson M, Smallwood R, Qwarnstrom E, et al. Formal agent-based modelling of intracellular chemical interactions. *Biosystems* 2006;**85**:37–45.
25. Pękalski J, Zuk PJ, Kochańczyk M, et al. Spontaneous NF-κB activation by autocrine TNFα signaling: a computational analysis. *PLoS One* 2013;**8**:e78887.
26. Turner DA, Paszek P, Woodcock DJ, et al. Physiological levels of TNFalpha stimulation induce stochastic dynamics of NF-kappaB responses in single living cells. *J Cell Sci* 2010;**123**:2834–43.
27. Stiles J, Bartol TM. Monte Carlo methods for simulating realistic synaptic microphysiology using MCell. In: Erik De Schutter (Ed.), *Computational Neuroscience*, Boca Raton, Florida: CRC Press, 2001, 87–127.
28. Andrews SS. Smoldyn: particle-based simulation with rule-based modeling, improved molecular interaction and a library interface. *Bioinformatics* Boca Raton, Florida: CRC Press, 2017;**33**:710–7.
29. Blinov ML, Schaff JC, Vasilescu D, et al. Compartmental and spatial rule-based modeling with virtual cell. *Biophys J* 2017;**113**:1365–72.
30. Michalski PJ, Loew LM. SpringSaLaD: a spatial, particle-based biochemical simulation platform with excluded volume. *Biophys J* 2016;**110**:523–9.
31. Chattaraj A, Youngstrom M, Loew LM. The interplay of structural and cellular biophysics controls clustering of multivalent molecules. *Biophys J* 2019;**116**:560–72.
32. Slepchenko BM, Schaff JC, Carson JH, et al. Computational cell biology: spatiotemporal simulation of cellular events. *Annu Rev Biophys Biomol Struct* 2002;**31**:423–41.
33. Slepchenko BM, Schaff JC, Macara I, et al. Quantitative cell biology with the virtual cell. *Trends Cell Biol* 2003;**13**: 570–6.
34. Francke C, Postma PW, Westerhoff HV, et al. Why the phosphotransferase system of Escherichia coli escapes diffusion limitation. *Biophys J* 2003;**85**:612–22.
35. Hattne J, Fange D, Elf J. Stochastic reaction-diffusion simulation with MesoRD. *Bioinformatics* 2005;**21**:2923–4.
36. Tomás-Oliveira I, Ferkinghoff-Borg J, Beltrao P, et al. SmartCell, a framework to simulate cellular processes that combines stochastic approximation with diffusion and localisation: analysis of simple networks. *Syst Biol (Stevenage)* 2004;**1**:129–38.
37. Rodriguez JV, Kaandorp JA, Dobrzynski M, et al. Spatial stochastic modelling of the phosphoenolpyruvate-dependent phosphotransferase (PTS) pathway in Escherichia coli. *Bioinformatics* 2006;**22**:1895–901.
38. Andrews SS, Bray D. Stochastic simulation of chemical reactions with spatial resolution and single molecule detail. *Phys Biol* 2004;**1**:137–51.
39. Ridgway D, Broderick G, Lopez-Campistrous A, et al. Coarse-grained molecular simulation of diffusion and reaction kinetics in a crowded virtual cytoplasm. *Biophys J* 2008;**94**:3748–59.
40. Frazier Z, Alber F. A computational approach to increase time scales in Brownian dynamics-based reaction-diffusion modeling. *J Comput Biol* 2012;**19**:606–18.
41. Lalani AI, Zhu S, Gokhale S, et al. TRAF molecules in inflammation and inflammatory diseases. *Curr Pharmacol Rep* 2018;**4**:64–90.
42. Kim CM, Choi JY, Bhat EA, et al. Crystal structure of TRAF1 TRAF domain and its implications in the TRAF1-mediated intracellular signaling pathway. *Sci Rep* 2016;**6**:25526.
43. Spit M, Rieser E, Walczak H. Linear ubiquitination at a glance. *J Cell Sci* 2019;**132**:jcs208512.
44. Kearns JD, Basak S, Werner SL, et al. IkappaBepsilon provides negative feedback to control NF-kappaB oscillations, signaling dynamics, and inflammatory gene expression. *J Cell Biol* 2006;**173**:659–64.
45. Zambrano S, de Toma I, Piffer A, et al. NF-κB oscillations translate into functionally related patterns of gene expression. *Elife* 2016;**5**:e09100.
46. Chen J, Sawyer N, Regan L. Protein-protein interactions: general trends in the relationship between binding affinity and interfacial buried surface area. *Protein Sci* 2013;**22**:510–5.
47. Qian H. Cooperativity in cellular biochemical processes: noise-enhanced sensitivity, fluctuating enzyme, bistability with nonlinear feedback, and other mechanisms for sigmoidal responses. *Annu Rev Biophys* 2012;**41**:179–204.
48. Liu T, Zhang L, Joo D, et al. NF-κB signaling in inflammation. *Signal Transduct Target Ther* 2017;**2**:17023.
49. Nussinov R. The spatial structure of cell signaling systems. *Phys Biol* 2013;**10**:045004.
50. Fu TM, Shen C, Li Q, et al. Mechanism of ubiquitin transfer promoted by TRAF6. *Proc Natl Acad Sci U S A* 2018;**115**:1783–8.
51. Huang B, Lu M, Jia D, et al. Interrogating the topological robustness of gene regulatory circuits by randomization. *PLoS Comput Biol* 2017;**13**:e1005456.
52. Xie Z-R, Chen J, Wu Y. A coarse-grained model for the simulations of biomolecular interactions in cellular environments. *J Chem Phys* 2014;**140**:054112.
53. Su Z, Wu Y. A computational model for understanding the oligomerization mechanisms of TNF receptor superfamily. *Comput Struct Biotechnol J* 2020;**18**:258–70.
54. Chen J, Almo SC, Wu Y. General principles of binding between cell surface receptors and multi-specific ligands: a computational study. *PLoS Comput Biol* 2017;**13**: e1005805.
55. Vanamee ÉS, Faustman DL. Structural principles of tumor necrosis factor superfamily signaling. *Sci Signal* 2018;**11**:eaao4910.
56. Zapata JM, Perez-Chacon G, Carr-Baena P, et al. CD137 (4-1BB) signalosome: complexity is a matter of TRAFs. *Front Immunol* 2018;**9**:2618.
57. Gillespie DT. Stochastic simulation of chemical kinetics. *Annu Rev Phys Chem*. 2007;**58**:35–55.
58. Chen J, Xie ZR, Wu Y. Elucidating the functional roles of spatial organization in cross-membrane signal transduction by a hybrid simulation method. *J Comput Biol* 2016;**23**: 566–84.